Refraction effects in soft x-ray multilayer blazed gratings

D. L. Voronov,* F. Salmassi, J. Meyer-Ilse, E. M. Gullikson, T. Warwick, and H. A. Padmore

Lawrence Berkeley National Laboratory, 1 Cyclotron Road, Berkeley, California 94720, USA
*dlvoronov@lbl.gov

Abstract. A 2500 lines/mm Multilayer Blazed Grating (MBG) optimized for the soft x-ray wavelength range was fabricated and tested. The grating coated with a W/B_4C multilayer demonstrated a record diffraction efficiency in the 2nd blazed diffraction order in the energy range from 500 to 1200 eV. Detailed investigation of the diffraction properties of the grating demonstrated that the diffraction efficiency of high groove density MBGs is not limited by the normal shadowing effects that limits grazing incidence x-ray grating performance. Refraction effects inherent in asymmetrical Bragg diffraction were experimentally confirmed for MBGs. The refraction affects the blazing properties of the MBGs and results in a shift of the resonance wavelength of the gratings and broadening or narrowing of the grating bandwidth depending on diffraction geometry. The true blaze angle of the MBGs is defined by both the real structure of the multilayer stack and by asymmetrical refraction effects. Refraction effects can be used as a powerful tool in providing highly efficient suppression of high order harmonics.

©2016 Optical Society of America

OCIS codes: (050.1950) Diffraction gratings; (340.7480) X-rays, soft x-rays, extreme ultraviolet (EUV).

References and links

1. W. Jark, "Enhancement of diffraction grating efficiencies in the soft x-ray region by a multilayer coating," Opt. Commun. **60**(4), 201–205 (1986).
2. J. C. Rife, W. R. Hunter, T. W. Barbee, Jr., and R. G. Cruddace, "Multilayer-coated blazed grating performance in the soft x-ray region," Appl. Opt. **28**(15), 2984–2986 (1989).
3. J. H. Underwood, C. Kh. Malek, E. M. Gullikson, and M. Krumrey, "Multilayer-coated echelle gratings for soft x-rays and extreme ultraviolet," Rev. Sci. Instrum. **66**(2), 2147–2150 (1995).
4. T. Warwick, Y.-D. Chuang, D. L. Voronov, and H. A. Padmore, "A multiplexed high-resolution imaging spectrometer for resonant inelastic soft X-ray scattering spectroscopy," J. Synchrotron Radiat. **21**(4), 736–743 (2014).
5. D. L. Voronov, L. I. Goray, T. Warwick, V. V. Yashchuk, and H. A. Padmore, "High-order multilayer coated blazed gratings for high resolution soft x-ray spectroscopy," Opt. Express **23**(4), 4771–4790 (2015).
6. D. L. Voronov, T. Warwick, and H. A. Padmore, "Multilayer-coated blazed grating with variable line spacing and a variable blaze angle," Opt. Lett. **39**(21), 6134–6137 (2014).
7. X. Yang, I. V. Kozhevnikov, Q. Huang, and Z. Wang, "Unified analytical theory of single-order soft x-ray multilayer gratings," J. Opt. Soc. Am. B **32**(4), 506–522 (2015).
8. D. Maystre and R. Petit, "Some recent theoretical results for gratings: application for their use in the very far ultraviolet region," Nouv. Rev. Opt. **7**(3), 165–180 (1976).
9. A. P. Lukirskii and E. P. Savinov, "Use of diffraction gratings and echelettes in the ultrasoft x-ray region," Opt. Spectrosc. **14**, 147–151 (1963).
10. A. P. Lukirskii, E. P. Savinov, and Y. P. Shepelev, "Behaviour of gold and titanium coated echelettes in the 23.6-113 A region," Opt. Spectrosc. **15**, 290–293 (1963).
11. M. Nevière and F. Montiel, "Soft x-ray multilayer coated echelle gratings: electromagnetic and phenomenological study," J. Opt. Soc. Am. A **13**(4), 811–818 (1996).
12. Y. Fujii, K. I. Aoyama, and J. I. Minowa, "Optical demultiplexer using a silicon echelette grating," IEEE J. Quantum Electron. **16**(2), 165–169 (1980).

#260326 Received 2 Mar 2016; revised 26 Apr 2016; accepted 27 Apr 2016; published 17 May 2016

13. P. Philippe, S. Valette, O. M. Mendez, and D. Maystre, "Wavelength demultiplexer: using echelette gratings on silicon substrate," Appl. Opt. **24**(7), 1006–1011 (1985).
14. D. L. Voronov, E. M. Gullikson, F. Salmassi, T. Warwick, and H. A. Padmore, "Enhancement of diffraction efficiency via higher-order operation of a multilayer blazed grating," Opt. Lett. **39**(11), 3157–3160 (2014).
15. http://henke.lbl.gov/multilayer/survey.htmlhttp://henke.lbl.gov/
16. http://henke.lbl.gov/optical_constants/multi2.html
17. http://www.pcgrate.com/
18. D. L. Voronov, E. H. Anderson, R. Cambie, S. Cabrini, S. D. Dhuey, L. I. Goray, E. M. Gullikson, F. Salmassi, T. Warwick, V. V. Yashchuk, and H. A. Padmore, "A 10,000 groove/mm multilayer coated grating for EUV spectroscopy," Opt. Express **19**(7), 6320–6325 (2011).
19. See, for example, Yu. Shvyd'ko, See, for example, Yu. Shvyd'ko, *X-Ray Optics. High-Resolution Applications*, (Springer, 2004).
20. V. V. Martynov and Yu. Platonov, "Deep multilayer gratings with adjustable bandpass for XRF spectroscopy," Adv. X-ray Anal. **45**, 402–408 (2002).
21. F. Choueikani, B. Lagarde, F. Delmotte, M. Krumrey, F. Bridou, M. Thomasset, E. Meltchakov, and F. Polack, "High-efficiency B_4C/Mo_2C alternate multilayer grating for monochromators in the photon energy range from 0.7 to 3.4 keV," Opt. Lett. **39**(7), 2141–2144 (2014).

1. Introduction

Multilayer Blazed Gratings (MBG) [1–3] offer great advantages in diffraction efficiency and dispersion over traditional grazing incidence x-ray diffractive optics due to their high groove density and high order operation. This enables the development of a variety of new high performance optical systems, such as ultra-high resolution spectrometers for Resonant Inelastic X-ray Scattering (RIXS) [4]. This revolutionary new spectroscopy is limited in terms of application by the requirement for extreme spectral resolution, and by the low RIXS cross section. Both limitations are essentially removed by use of MBG optics.

However, MBG bandwidth at a fixed incidence angle is limited by the relatively narrow Bragg reflection from the multilayer. This requires careful optimization of the grating design to match the resonance wavelength of a MBG to a target value, for example, to a specific x-ray absorption edge in the RIXS experiment. This calls for a deep understanding of the diffraction of x-rays in the multilayer stack of a MBG.

Diffraction properties of soft x-ray MBGs were recently investigated via numerical simulations [5,6] and analytically [7]. The simulations revealed that refraction effects inherent to asymmetrical Bragg diffraction should be taken into account when a grating is designed. The asymmetrical refraction effects are negligible for EUV MBGs operating at normal incidence but are crucial for soft x-ray gratings which operate at oblique illumination where refraction is substantial and can alter bandwidth and diffraction efficiency significantly.

Using a simple scalar mode Maystre and Petit [8] showed that the diffraction efficiency of blazed gratings is a product of the reflectance of the surface of the blazed facets, R, and an asymmetry factor which depends on the diffraction geometry:

$$E_{Maystre} = R \times \min\left[\cos\alpha / \cos\beta, \cos\beta / \cos\alpha\right], \tag{1}$$

where α and β are incidence and diffraction angles respectively. The geometry factor describes a shadowing effect [9,10] and is equal to the fraction of the wavefront which falls on the non-shadowed part of the grating groove and can therefore contribute to a blazed order by "specular reflection" from the blazed facet surface. The shadowing effect determines the relative efficiency of a diffraction grating which is the ratio of the absolute efficiency to the surface reflectance, E/R. The phenomenological formula (1) was found to work well as a good approximation for the efficiency of grazing incidence x-ray gratings and later on was confirmed for low groove density multilayer blazed gratings [11] if the surface reflectance in formula (1) is replaced by the ML reflectance. However, we found by numerical simulations that this is not always the case. For multilayer blazed gratings with very high groove density, when the grating pitch is smaller than the penetration length of the x-rays, the multilayer grooves become semi-transparent and the shadowing effect is dramatically relaxed. As a result, the diffraction efficiency is expected to be significantly higher than the value predicted

#260326 Received 2 Mar 2016; revised 26 Apr 2016; accepted 27 Apr 2016; published 17 May 2016
© 2016 OSA

by formula (1). On the other hand, the diffraction efficiency of an ultra-dense multilayer grating is affected by refraction in the multilayer which in turn depends on the diffraction geometry [5].

All of these unique properties of MBGs were discovered via numerical simulations and therefore require experimental verification. In this work we report for the first time on the fabrication of a highly efficient soft x-ray MBG and on the investigation of its diffraction properties in order to verify the predictions of simulations. In this work we investigate, (1) the dependence of the relative efficiency of MBGs on the diffraction geometry, (2) the dependence of the MBG bandwidth on the diffraction geometry, (3) the impact of refraction on the blazing properties of MBGs, and (4) the suppression of high harmonic diffraction in MBGs.

2. Experimental

A saw tooth substrate with a target groove density of 2500 lines/mm and a blaze angle of 2° was fabricated by anisotropic wet etching of a silicon single crystal as described elsewhere [12–14].

A W/B_4C multilayer was chosen as a high-reflectivity coating for the soft x-ray grating since it has the highest reflectance in the 500eV-1500eV energy range [15]. Parameters of the saw-tooth substrate and the multilayer were chosen to provide a blazed effect for the 2nd diffraction order of the MBG. The multilayer was composed of 18 bi-layers deposited on the saw-tooth substrate and in addition a witness multilayer was deposited on a plane silicon substrate. DC-magnetron and RF-magnetron sources were used to sputter W and B_4C targets respectively.

Measurements of grating efficiency and multilayer reflectance were performed at the Advanced Light Source x-ray synchrotron using a two axis reflectometer on beamline 6.3.2. Reflectance of the witness multilayer were measured by monochromator scans at fixed grazing angles in the range 5°-16°.

Absolute efficiency of the MBG in a wide range of wavelengths was measured by monochromator scans at incidence angles α = 75.5°-85.8° from the normal to the grating surface (which corresponds to grazing angles of 3.8° - 14.5° with respect to the grating plane) for the positive (inside) order diffraction where $|\alpha|>|\beta|$. Such geometry will be referred to in the following as the direct geometry. The negative (outside) order diffraction when $|\alpha_r|<|\beta_r|$ and $|\alpha_r| = |\beta|$, $|\beta_r| = |\alpha|$ will be referred to as a reciprocal geometry. The incidence angles for the reciprocal geometry were in the range of α_r = 72°-83°.

In order to investigate the distribution of the diffracted energy among different diffraction orders, detector scans over a range of diffraction angles were performed for different incident angles and wavelengths. A 0.5 mm wide detector slit was used for these measurements to resolve the diffraction orders.

Simulations of soft x-ray reflectance of the multilayer witness were performed using the standard recursive method used in the CXRO database [16].The multilayer parameters such as the d-spacing obtained by the fitting of soft x-ray reflectance curves are in good agreement with x-ray reflectometry at a wavelength of 0.154 nm.

Simulations of the diffraction efficiency of the grating were performed with a commercial electromagnetic field simulation code (PCGrate 6.5) based on the rigorous boundary integral formulation [17]. The code allows calculation of the efficiency of diffraction gratings having an ideal or realistic groove profile and coated with a metal coating or a multilayer with ideal interfaces.

#260326 Received 2 Mar 2016; revised 26 Apr 2016; accepted 27 Apr 2016; published 17 May 2016
© 2016 OSA

3. Results and discussion

3.1. Diffraction efficiency

Figure 1 shows an AFM image and a saw-tooth profile of the coated grating. Grating grooves have an almost perfect triangular shape with a blaze angle of 1.76° ± 0.02°, and an antiblaze angle of about 20°. The blaze angle is the same as for the saw-tooth substrate before the deposition and somewhat different from the target angle of 2°. The deviation is within +/–0.5° tolerances for the Si substrate orientation.

Absolute efficiency measured at incidence angles in the range 75.7°-85.8° degrees is shown in Fig. 2 along with theoretical efficiency curves calculated for the respective geometries. The calculations were performed for the experimental groove profile measured by AFM and assuming ideally smooth and sharp interfaces of the multilayer. The difference between the calculated and measured efficiency is caused by multilayer interface imperfections as well as imperfection of the saw-tooth substrate.

To calculate experimental relative efficiency and compare it to the formula (1) we need to pay attention to the thickness of interfaces of the multilayer, which includes both roughness and interdiffusion of the materials at the interfaces. The interface thickness of a plane W/B4C multilayer can be estimated from measurements of reflectance of the multilayer witness (Fig. 3(a)). The ML witness was deposited on a Si substrate with a surface roughness of 0.09 nm rms measured over a scan area of 5 μm × 5 μm. Roughness of the top surface of the multilayer was measured to be 0.08 nm. Since there is no significant change of the roughness before and after deposition we can assume that internal interfaces of the ML stack have the same roughness of ~0.08 nm. Fitting of the ML reflectance curves yields an interface thickness of σ = 0.46 nm rms which is much higher than roughness measured by AFM, indicating that intermixing of materials at the interfaces is a major factor in interface blurring. The contribution of the interdiffusion to the interface thickness can be estimated as σ_{diff} = 0.45 nm rms for the plane witness multilayer assuming Gaussian distribution of the quantities $\sigma^2 = \sigma^2_{rough.} + \sigma^2_{diff.}$. The impact of the interface imperfections on the ML reflectance is shown in Fig. 3(b) where experimental reflectance (triangle symbols) is compared to the reflectance of an ideal multilayer with smooth and sharp interfaces (blue curve). The red curve shows calculated reflectance for interface thickness of σ = 0.46 nm rms.

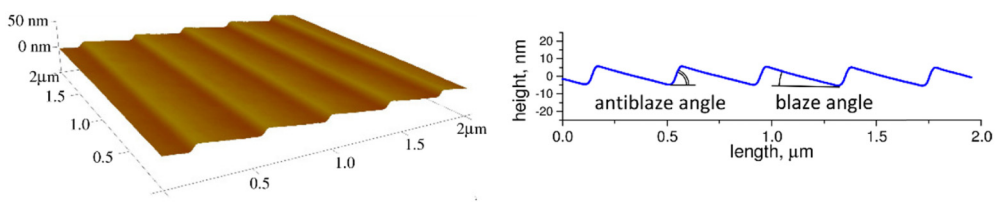

Fig. 1. An AFM image (left) and profile (right) of the 2,500 lines/mm soft x-ray multilayer blazed grating.

#260326 Received 2 Mar 2016; revised 26 Apr 2016; accepted 27 Apr 2016; published 17 May 2016
© 2016 OSA

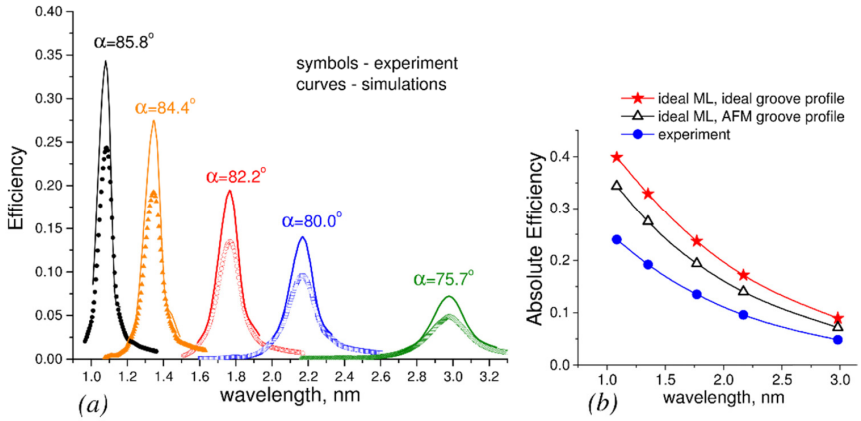

Fig. 2. Efficiency of the soft x-ray MBG versus wavelength measured (symbols) and calculated (curves) for different incidence angles (a). Experimental (curve with circles) and theoretical peak diffraction efficiency calculated for anti-blaze angles of 20° (curve with triangles) and 80° (curve with star symbols) (b).

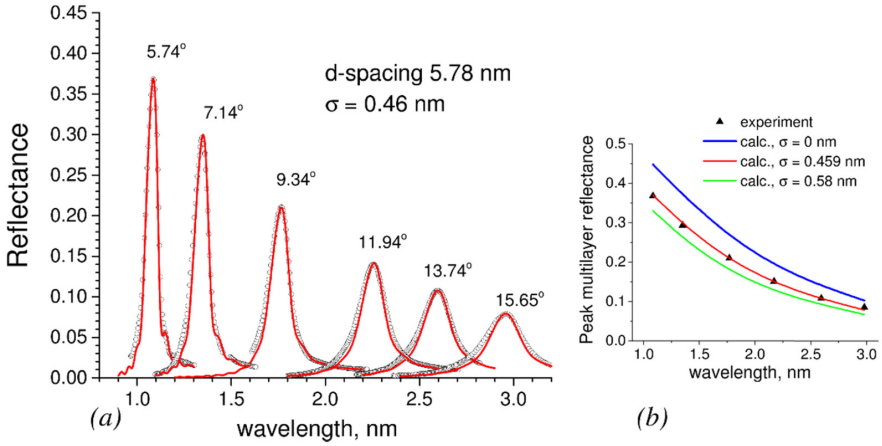

Fig. 3. Reflectance of the W/B4C plane multilayer witness versus wavelength measured (circles) and calculated (curves) for different grazing angles of incidence (a). Experimental and theoretical peak ML reflectance calculated for interface roughness of 0, 0.46, and 0.58 nm rms (b).

The reflectance of the multilayer deposited on the saw-tooth substrate is expected to be somewhat lower as compared to the plane witness multilayer due to the difference in interface thickness. Roughness of 0.36 nm rms was measured for the saw-tooth substrate over a scan area of 5 μm × 5 μm before deposition and the same for the top surface of the blazed grating after deposition. Again there is no significant changes of the interface roughness during the deposition and the interface roughness is defined by the substrate imperfections. Combining the interface roughness with interfusion broadening of 0.45 nm found for the witness one can estimate the total interface thickness as σ = 0.58 nm rms for the multilayer deposited on the saw-tooth substrate. The reflectance of such a multilayer is shown in the green curve in Fig. 3(b). These reflectance data will be used for calculation of the relative efficiency of the multilayer grating which is the ratio of the absolute diffraction efficiency of the grating to the reflectance of the plane multilayer with an interface thickness of 0.58 nm.

Blurred interfaces result in a reduction of the reflectance as compared to ideal interfaces (the blue curve in Fig. 3(b)) by a factor of 1.4 – 1.5. This is very close to the ratio of calculated and experimental efficiency of the grating (curves with triangles and circles in Fig.

#260326 Received 2 Mar 2016; revised 26 Apr 2016; accepted 27 Apr 2016; published 17 May 2016
© 2016 OSA

2(b)) pointing out that the difference is caused mostly by the multilayer interface imperfections. Note that an ideal grating with short 80-degree tilted anti-blazed facets would have higher efficiency (the curve with star symbols in Fig. 2(b)). Although it is possible to achieve very steep facets for the saw tooth substrate by anisotropic wet etch, it is challenging to preserve the profile during multilayer deposition due to smoothing effects [18].

Now we can compare relative efficiency calculated by the phenomenological formula (1) to the experimental one for different asymmetry parameters. The phenomenological relative efficiency is just equal to the asymmetry parameter and linearly reduces with asymmetry (i.e. for low cosα/cosβ values) while the experimental one demonstrates a completely different behavior being almost independent of the asymmetry parameter. The same tendency is clearly seen for the efficiency of the ideal grating calculated using the PCGrate code. Here the relative efficiency was calculated as the ratio of absolute diffraction efficiency of the ideal grating (see the curve with star symbols in Fig. 2(b)) to the ideal multilayer reflectance (see the blue curve in Fig. 3(b)) computed using CXRO simulation code [16]. The relative efficiency of an ideal grating with the anti-blaze angle of 80° is almost independent of the asymmetry parameter and approaches 90% (the curve with star symbols in Fig. 4), much higher than the experimental value. More realistic simulations using the experimental groove profile measured by AFM (See Fig. 1) yield relative efficiency consistent with the experimental one (the curve with triangle symbols in Fig. 4). The fact that the efficiency does not depend linearly on the asymmetry parameter and can significantly exceed the phenomenological one is direct proof that the shadowing effect is significantly relaxed for the ultra-short MBGs due to the semi-transparency of the short multilayer grooves and is not a limiting factor for the diffraction efficiency of ultra-dense multilayer gratings.

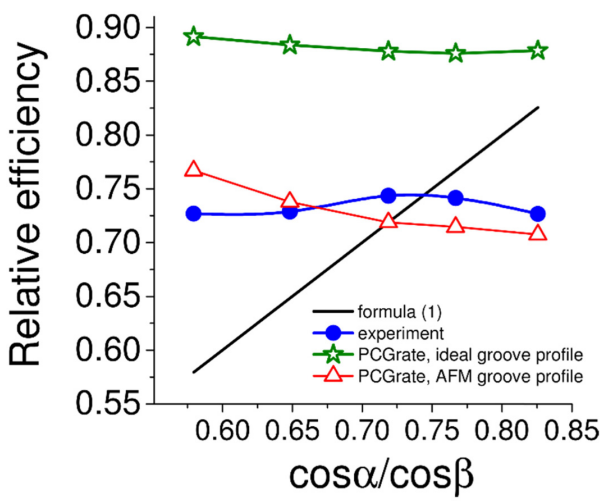

Fig. 4. Relative efficiency versus the asymmetry factor: calculated by formula (1), experimental, and calculated by PCGrate 6.5 code for an ideal grating with the anti-blaze angle 80° and a grating with realistic groove profile measured by AFM (see Fig. 1).

3.2. Bandwidth

In previous work [5] we found via simulations that refraction effects inherent to asymmetrical Bragg diffraction [19] are relevant to MBGs. They affect diffraction efficiency and bandwidth of the gratings and their impact depends on diffraction geometry. In this and following sections we provide experimental proof of the specific refraction effects in MBGs.

The efficiency curves in Fig. 2(a) show bandwidths of the grating measured in the direct geometry when $|\alpha| > |\beta|$. We also performed measurements of the same grating in the reciprocal geometry when the incidence and diffraction angles were switched over and $|\alpha_r| <$

#260326 Received 2 Mar 2016; revised 26 Apr 2016; accepted 27 Apr 2016; published 17 May 2016
© 2016 OSA

$|\beta_r|$ and the efficiency of the 2nd negative order was measured. One pair of the direct/reciprocal curves for the incidence angles of 80° and 76.88° respectively is shown in Fig. 5(a). Both the measurements yielded the same resonance wavelength of 2.17 nm and the same peak efficiency of about 9.4% while the width of the efficiency curves is different. The full width at half maximum (FWHM) of 0.18 nm and 0.14 nm of the curves represents an almost 29% narrowing of the grating bandwidth for the reciprocal geometry as compared to the direct one.

The difference in the bandwidths is systematically observed for the reciprocal geometry in the whole wavelength range as shown in Fig. 5(b) where the FWHM for the direct and reciprocal geometry are plotted along with the bandwidth of the plane multilayer witness. It is seen that the direct geometry diffraction results in a broadening of the bandwidth while the reciprocal geometry leads to a narrowing of the grating bandwidth as compared to the plane multilayer.

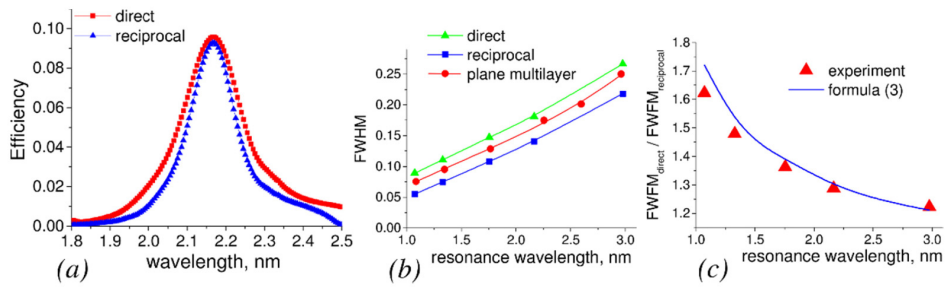

Fig. 5. Efficiency of the fabricated multilayer grating measured for the direct (α = 79.96°) and reciprocal (α_r = 76.88°) geometry (a). Dependence of the bandwidth for a plane multilayer witness (circles) and the grating in direct (triangles) and reciprocal (squares) geometry (b). Experimental (symbols) and calculated by formula (3) (curve) ratio of the bandwidths for direct and reciprocal geometry (c)

The narrowing factor defined as $FWHM_{direct}/FWHM_{reciprocal}$ ranges from 1.2 to 1.6 for the wavelengths of 3 nm and 1 nm respectively (Fig. 5(c)). Such a bandwidth behavior corresponds to asymmetrical Bragg diffraction which is known to manifest significant refraction effects. According to the dynamic theory, the spectral width of total Bragg reflection for crystals depends on the asymmetry as:

$$FWHM_a = FWHM_S / \sqrt{|b|} \tag{2}$$

where $FMHM_s$ and $FMHM_a$ are bandwidths for symmetrical and asymmetrical diffraction respectively, and b is an asymmetry parameter which in the grating notation can be written as $b = -\cos\alpha/\cos\beta$ for the direct geometry and $b = -\cos\alpha_r/\cos\beta_r = -\cos\beta/\cos\alpha$ for the reciprocal geometry. The ratio of the asymmetrical bandwidths for the direct and reciprocal geometry can be found as:

$$FWHM_a^{direct} / FWHM_a^{reciprocal} = |b| = \cos\beta / \cos\alpha \tag{3}$$

The narrowing factors calculated with formula (3) are in good agreement with those experimentally observed (Fig. 5(c)). This is direct experimental evidence of the applicability of asymmetrical Bragg diffraction to diffraction in MBGs.

3.3. True blaze angle

The high efficiency of blazed gratings is achieved by a tilt of the groove facets so that most of the energy is concentrated in the blazed diffraction order while all other orders are suppressed. For regular reflective gratings, the angle of the tilt is chosen so that diffraction into the blazed

#260326 Received 2 Mar 2016; revised 26 Apr 2016; accepted 27 Apr 2016; published 17 May 2016
© 2016 OSA

order corresponds to specular reflection of the incidence beam from the facet surface, which leads to the definition for the blaze angle

$$\phi = (\alpha - \beta)/2 \tag{4}$$

This is however not exactly true for multilayer gratings due to refraction effects caused by asymmetric Bragg diffraction. The reflectance from a multilayer is a bulk process and involves refraction which modifies the Bragg reflection for plane multilayers. In MBGs refraction is more complicated due to asymmetry of the diffraction. In this section we investigate how refraction modifies the blaze condition of the fabricated multilayer grating.

Figure 6 shows a detector scan at a wavelength of 1.77 nm, corresponding to the maximum of the efficiency curve for an incidence angle of 82.2° (Fig. 2(a)). The diffraction pattern consists of a strong blazed 2nd order diffraction peak and a few very weak peaks which are non-blazed orders including the zero order. The latest verifies the incidence angle of 82.2°. The3rd order diffraction peak is the strongest among the non-blazed ones and results from small deviation of the ML d-spacing from an ideal one as will be discussed below. The vast majority of the light however is diffracted into 2nd order. The grating period value of 401.7 nm calculated from the diffraction data is consistent with AFM measurements of 403.3 nm with a negligible discrepancy of 0.4% which confirms good calibration of xyz-scanner of AFM. Since the diffraction angle for the 2nd order is 79.1° the effective blaze angle calculated with formula (4) is 1.55° which is significantly different from the blazed facet tilt angle of ϕ_0 = 1.76° measured by AFM for the saw-tooth substrate. The difference is caused by two reasons as will be discussed below: 1) a staggered structure of the ML stack and 2) the asymmetrical refraction effects.

Since the blaze condition of a MBG is defined by both the grating Eq. and the Bragg condition, it depends on parameters of both the saw-tooth substrate and the multilayer. An ideal blazing is achieved when the substrate and multilayer parameters are coupled as follows [2, 3]:

$$\frac{d_{grating} \sin\phi_0}{D_{ML}} = \frac{m}{n}, \tag{5}$$

which shows that the ratio of the substrate groove depth defined as $d_{grating} \times \sin\phi_0$ to the ML d-spacing, D_{ML}, should be equal to the ratio of a diffraction order, m, and a Bragg order, n, and is an integer number for normally used n = 1. For the grating with period d = 401.7 nm, blaze angle of 1.76°, and the 1st order Bragg diffraction, n = 1, the optimal d-spacing of the multilayer should be of 6.17 nm and 4.11 nm for the 2nd and 3rd order blazing respectively. The real d-spacing of the ML deposited on the grating was 5.78 nm which is close to the 2nd blazed order slightly towards the 3rd order condition. As a result of this, part of the diffracted energy goes to the 3rd diffraction order which is the strongest one among other non-blazed orders in (Fig. 6). The strong 2nd blazed order and a fairly weak 3rd order was observed in the whole wavelength range investigated in this paper (Fig. 6(b)) since the blaze condition (5) does not depend on a wavelength or angle of incidence.

#260326 Received 2 Mar 2016; revised 26 Apr 2016; accepted 27 Apr 2016; published 17 May 2016
© 2016 OSA

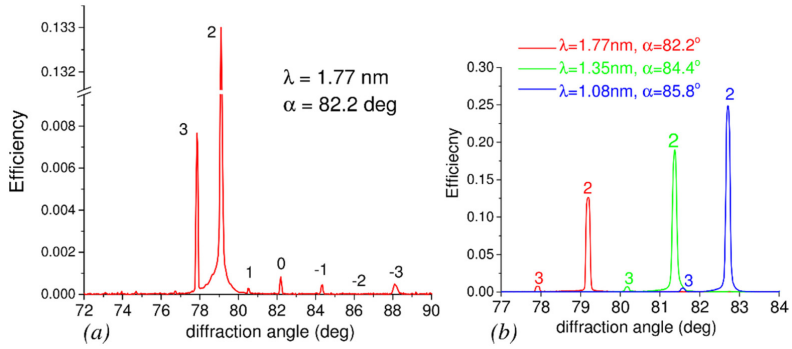

Fig. 6. Detector scan for the incidence angle of 82.2° and the wavelength of 1.77 nm (a). The same for a range of the wavelengths (b).

The deviation of the ML d-spacing from the one defined by formula (5) prevents perfect stitching of the layers resting on adjacent grooves and results in staggered interfaces of the multilayer as was discussed elsewhere [6]. The periodic structure of such a multilayer stack composed of the staggered layers has a slightly different d-spacing and what is more important, a different slope which defines a true blaze angle (see Fig. 7):

$$tg\phi = \frac{D_{ML} m}{d_{grating} \cos\phi_0}, \tag{6}$$

According to formula (6), the real tilt of the staggered layers in the grating considered in this paper is 1.65° while the tilt angle of the saw-tooth substrate facets is 1.76°. The difference is substantial since it affects the Bragg condition and hence the grating resonance wavelength significantly.

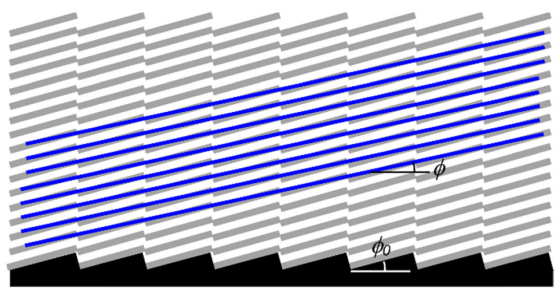

Fig. 7. A structure of a MBG with slight deviation from the ideal blazing condition (formula (5)). Staggered layers define a new periodical structure with an effective blaze angle, ϕ, different from the substrate blaze angle, ϕ_0.

In terms of the true blaze angle of 1.65°, the incident Bragg angle is θ_B^{in} = 90°-α + ϕ = 90°-82.2° + 1.65° = 9.45° for the diffraction at the wavelength of 1.77 nm (Fig. 6(a)). At the same time the Bragg angle for the diffracted beam is θ_B^{out} = 90°-β -ϕ = 90°-79.1° –1.65° = 9.26°. This experimental difference between the Bragg angles for the incident and diffracted waves should be explained along with a shift of the MBG resonance wavelength as compared to the resonance wavelength of the same multilayer deposited on a plane substrate. Indeed, for a d-spacing of 5.78 nm, and Bragg angle of 9.45°, the resonance wavelength of the multilayer calculated by [16] is 1.794 nm which is quite different from the experimental resonance wavelength of 1.77 nm of the grating. These experimental facts can be explained by the dynamical theory for asymmetrical Bragg diffraction [19].

Following [19] the Bragg Eq. can be modified to take into account refraction as:

#260326 Received 2 Mar 2016; revised 26 Apr 2016; accepted 27 Apr 2016; published 17 May 2016
© 2016 OSA

$$2D\sin\theta = n\lambda(1+\omega_S), \quad (7)$$

where ω_s is a correction term for symmetrical refraction. For a d-spacing of 5.78 nm, and a Bragg angle of 9.45°, the resonance wavelength of the multilayer is 1.794 nm and the symmetrical refraction correction term calculated by formula (7) is $\omega_s = 0.0577$. In the case of asymmetrical diffraction, the symmetrical refraction correction term in formula (7) should be replaced by the asymmetrical term, ω_a, which can be found from $\omega_a = \omega_s(b-1)/(2b)$ for the incident wave. For the asymmetry parameter b = - cos82.2°/cos79.1° = - 0.7177, the asymmetrical correction term is $\omega_a = 0.0690$ and the resonance wavelength of the multilayer grating is 1.775 nm which is in a good agreements with the experimental value of 1.77 nm. For the exit wave the asymmetry correction is $\omega_a = \omega_s(1-b)/2 = 0.0496$, and the exit Bragg angle for the resonance wavelength of 1.77 nm is 9.25° which is in excellent agreement with the experimental value of $\theta_B^{out} = 9.26°$. We conclude that asymmetrical Bragg diffraction theory provides quantitative explanation of both the shift of the resonance wavelength and non-specular Bragg reflection.

The fact that "in" and "out" angles are not exactly the same means that the condition of "specular reflection" from the blaze interfaces is not the case for MBGs. This explains the difference between the true blaze angle of 1.65° and an apparent blaze angle of 1.55° for the diffraction shown in Fig. 6. This deviation from the specular reflection can compromise the blazing ability of MBGs and seems to be the main reason for reduction of the theoretical diffraction efficiency observed for $\alpha \to 90°$ or $\beta \to 90°$ when refraction is strongest [5].

3.4. High harmonic suppression in MBGs

Spectral purity is one of the concerns regarding grating monochromators for EUV and soft x-ray light. Since the diffraction angles for a certain grating groove density and an incidence angle are defined by the product of mλ, high order harmonics λ/2, λ/3 etc. come through the exit slit of the monochromator along with a desirable wavelength λ. It is possible to control the high harmonics by a proper choice of grazing angles in plane grating monochromators or by high order suppressor devices, but always at the expense of throughput.

Unlike grazing incidence gratings MBGs can provide effective high order suppression without any additional optics. Although formula (5) gives a blaze condition for all diffraction orders with the same m/n ratio, the efficiency of higher harmonics defined by high order Bragg diffraction is usually low. Figure 8(a) shows the efficiency of the 2nd, 4th, and 6th blazed orders of the MBG measured at the incidence angle of 75.7°. Efficiency of the 4th and 6th orders is smaller than efficiency of the 2nd order by a factor of 6 and 50 respectively. Attenuation of high harmonics is caused partially due to blurred interfaces of the ML which affects the high Bragg orders exponentially according to the Debye –Waller factor. Moreover, some Bragg reflections can be weakened or completely suppressed for a certain Γ-ratio of the multilayer which is the ratio of thickness of a heavy material layer to the d-spacing. For example, even Bragg orders are suppressed for Γ = 0.5, and 3rd, 6th etc. orders are suppressed for Γ = 0.3.

An additional high harmonic suppression comes from the refraction in the multilayer as demonstrated in Fig. 8(b). Here the efficiency curves from Fig. 8(a) are normalized to have the same height and are plotted versus the product of the wavelength and the diffraction order. One can see that the high order efficiency curves are shifted with respect to the 2nd order bandwidth. The shift is caused by refraction in the multilayer which depends on wavelength. This means that the resonance wavelengths of high diffraction orders are not overtones of the 2nd order resonance wavelength and diffraction angles corresponding to maximum of the efficiency curves are substantially different. For the example shown in Fig. 8(b) the diffraction angles are 72.59°, 72.47°, and 72.42° for m = 2, 4, and 6 respectively. The angle separation of 2.2 mrad between 2nd and 4th orders and 3.0 mrad between the 2nd and 6th orders will result in spatial separation of 2.2 mm and 3.0 mm at the image plane of a

#260326 Received 2 Mar 2016; revised 26 Apr 2016; accepted 27 Apr 2016; published 17 May 2016
© 2016 OSA

monochromator with the exit arm of 1 meter. Here the high diffraction orders can be easily blocked by the exit slit and only small portion of high harmonics light corresponding to tails of their bandwidths can go through. In this way the bandwidth shift provides additional suppression of the 4th and 6th diffraction orders by a factor of 10 and 35 respectively. The total suppression in terms of Debye –Waller factor would be 60 and 1700 respectively.

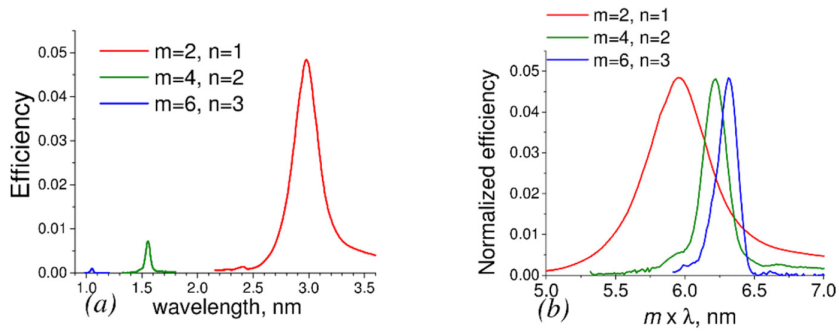

Fig. 8. Diffraction efficiency of the 2nd, 4th, and 6th blazed orders of the MBG measured at an incidence angle of 75.7° (a). Normalized efficiency of the 2nd, 4th, and 6th orders versus a product of the wavelength and diffraction order (b).

Summary

High efficiency multilayer blazed gratings optimized for soft x-rays including the effects of refraction were fabricated and tested for the first time. We obtain direct experimental proof that diffraction in MBGs follows dynamical theory for asymmetrical Bragg diffraction. Refraction effects inherent in the asymmetrical case affect the resonance wavelength of the MBGs and result in broadening or narrowing of the grating bandwidth for the direct and reciprocal diffraction geometry respectively. The asymmetrical refraction effects results in deviation of Bragg diffraction from specular geometry and results in a change of the apparent blaze angle of MBGs. These effects can be used as a powerful tool to suppress unwanted harmonics. The refraction effects discovered for MBGs are expected for any multilayer-coated gratings including lamellar multilayer gratings [20,21]. Refraction should be considered carefully for the design of multilayer grating based x-ray instrumentation.

Acknowledgments

This document was prepared as an account of work sponsored by the United States Government. While this document is believed to contain correct information, neither the United States Government nor any agency thereof, nor The Regents of the University of California, nor any of their employees, makes any warranty, express or implied, or assumes any legal responsibility for the accuracy, completeness, or usefulness of any information, apparatus, product, or process disclosed, or represents that its use would not infringe privately owned rights. Reference herein to any specific commercial product, process, or service by its trade name, trademark, manufacturer, or otherwise, does not necessarily constitute or imply its endorsement, recommendation, or favoring by the United States Government or any agency thereof, or The Regents of the University of California. The views and opinions of authors expressed herein do not necessarily state or reflect those of the United States Government or any agency thereof or The Regents of the University of California.

Advanced Light Source and Molecular Foundry are supported by the Director, Office of Science, Office of Basic Energy Sciences, of the U.S. Department of Energy under Contract No. DE-AC02-05CH11231.